Ultrafine Magnetic Particles: A DIET-Proxy in Organic Rich Sediments?

Andrea Teixeira Ustra[1]*, Carlos Mendonça[1], Aruã da Silva Leite[2,3], Melina Macouin[2,3], Rory Doherty[4], Marc Respaud[2,5] and Giovana Tocuti[1]

[1]Department of Geophysics, University of São Paulo, São Paulo, Brazil, [2]Université de Toulouse, Toulouse, France, [3]GET/OMP, UMR CNRS 5563, Université Paul-Sabatier, Toulouse, France, [4]School of Natural and Built Environment, Queen's University Belfast, Belfast, United Kingdom, [5]LPCNO-INSA Toulouse, CNRS, CEMES, UPR 8011, Université de Toulouse, Toulouse, France

In this work we present results of the magnetic properties characterization of sediment samples from a brownfield site that is generating methane biogas in São Paulo–Brazil. We applied interpretation procedures (frequency dependent susceptibility and time-dependent Isothermal Remanent Magnetization) appropriate to study the ultrafine magnetic fraction response of the samples. The higher content of superparamagnetic (SP) particles correlates well with the detected biogas pockets, suggesting that the methanogens activity produces these ultrafine particles, different from the magnetic particles at other depth levels. We propose the use of two simple measurement and interpretation techniques to identify such magnetic particles fingerprints. The results presented here support the use of environmental magnetism techniques to investigate biogeochemical processes of anaerobic microbial activity.

Keywords: direct inter species electron transfer (DIET), magnetic nanoparticles, superparamagnetic particles, methane, brownfield, organic rich sediments

INTRODUCTION

Organic matter buried in anaerobic environments, (e.g. landfills or organic-rich sediments) is oxidized through a series of biogeochemical processes producing methane and carbon dioxide as major products (Christensen, 2010). The well-known electron sources for carbon dioxide reduction to methane are H_2 (Sieber et al., 2012) or other dissolved carriers (Bryant et al., 1967; Stams and Plugge, 2009). Recent findings however have shown that *Methanosaeta* and *Methanosarcina* species can directly accept electrons from *Geobacter* as donors via direct interspecies electron transfer (DIET), in this process reducing carbon dioxide to methane (Chen et al., 2014a; Rotaru et al., 2014a; Chen et al., 2014b; Rotaru et al., 2014b; Wang et al., 2016; Xiao et al., 2018). Possible mechanisms of electron transfer in DIET-based syntrophy seem to be through electrified paths formed by pili-like appendages with conductive minerals or outer cell electrical connectors of adjacent partners (Lovley, 2017). DIET connection of *Methanosaeta* with *Geobacter* species has been recognized (Summers et al., 2010; Lovley, 2011; Shrestha et al., 2013a; Shrestha et al., 2013b) and assumed as a major player in global methane budget (Rotaru et al., 2014b). Methane production based on DIET can be stimulated by introducing conductive particulates (Martins et al., 2018), such as biochar (Chen et al., 2014a; Xiao et al., 2019); carbon cloth (Li et al., 2018) and magnetite nanoparticles (Kato et al., 2012; Zhang and Lu, 2016; Xiao et al., 2018) suggesting the importance of conductive particulate to shuttle interspecies electron-transport.

In principle, syntrophic DIET associations can sustain methanogenesis in H_2 depleted environments (or other dissolved carriers) by directly coupling iron-reducing bacteria with methanogens. It is accepted that the partnership between *Geobacter* and *Methanosarcina* can competitively exclude acetoclastic methanogens like *Methanothrix* in the absence of dissolved electron carrier (Rotaru et al., 2018). Paddy soil incubation of ferrihydrite indicates that methanogenesis is initially suppressed as magnetite grains are produced and *Geobacter* proliferates, and then enhanced as DIET develops using the magnetite network for interspecies electrical connections (Liu et al., 2015). Other species such as *Syntrophomonas* have been proposed as candidates for DIET with *Methanosaeta* suggesting that many microorganisms are capable of DIET processes (Zhao et al., 2018).

Magnetite production and alteration then may develop a major role in DIET syntrophy, either in stages in which Fe(III) reduction are catalyzed by iron-reducing bacteria as used to convey electron-transfer between interspecies partners. Iron speciation by dissimilatory iron-reducing bacteria is widespread in waterlogged soils (Lovley et al., 1987; Maher and Taylor 1988) and their importance for iron cycling in such environments makes them a key potential source of ultra-fine soil magnetite (Roberts, 2015). A proxy characterizing concentration and magnetite properties (grain size and mineral type, for example) may be useful to recognize a biogeochemical process active in modern environments or recorded in continuous coring of sedimentary sequences. A diversity of iron-reducing microorganisms can convert poorly crystalline Fe(III) oxy/hydroxides to extracellular magnetite while using Fe(III) as an electron acceptor for the oxidation of organic compounds (Lovley et al., 2004). The Fe (III) reducing bacteria *Geothrix* has been shown to produce magnetite at brownfield sites (Klueglein et al., 2013) and it has been suggested the Geothrix can act in syntrophy with methanogens though not necessarily via a DIET mechanism (Sutcliffe et al., 2018). Common Fe(III) minerals in soils and sediments are hematite (α-Fe_2O_3), ferrihydrite ($5Fe_2O_3.9H_2O$) or oxyhydroxides goethite (α-FeOOH), lepidocrocite (γ-FeOOH). The reduction of Fe(III) minerals to produce magnetite (Fe_3O_4) is energetically favorable ($\sim$0.01 eV), adding 1 Bohr magneton (9.27×10^{-24} Am^2) to the crystalline frame, which represents a magnetization upgrade of about 25% (Liu et al., 2012).

Depending on culture conditions and bacterial forms (Vali et al., 2004), the respiration of iron-reducing bacteria based on solid Fe(III) mineral phases produces extracellular magnetite crystals (Lovley et al., 1987; Lovley, 1991; Coker et al., 2008) of ultrafine grains with diameters between 10 and 50 nm. The extracellular crystallization process results in particles lacking characteristic morphology but usually with superparamagnetic (SP) properties at room temperature (Moskowitz et al., 1993). The superparamagnetic response is observed when single-domain, ferromagnetic minerals are below a critical blocking volume, unable to sustain permanent magnetization at room temperature. Incubation of metal-reducing bacteria with Fe(III) oxyhydroxides have produced magnetite nanoparticles with diameters between 10 and 15 nm for bacterium *Geobacter sulfurreducens* (Byrne et al., 2015) and between 26 nm and 38 nm for bacterium *Shewanella* (Lee et al., 2008). In many environments the magnetic properties associated to ultrafine magnetite particles must be isolated in order to better understand the superparamagnetic signature associated to iron-reducing bacteria and their role in DIET syntrophy.

In this paper we study a trapped gas pocket formed in Quaternary organic sediments, by tracking specific mineral changes that can be associated to biogeochemical processes. We focus our analysis on changes regarding the magnetic carrier mineralogy analyzing the frequency dependent susceptibility and time-dependent Isothermal Remanent Magnetization (IRM) to detect subtle physical and compositional variations that could be indicative of a DIET process. In addition to classic techniques used in environmental magnetism (thermomagnetic and hysteresis curves) we apply specific procedures to characterize the SP mineral content in terms of volume variations and concentration estimates along a cored section that intercepts a methane pocket trapped within organic-rich sediments. We recognize an association between iron-reducing bacteria and occurrence of SP minerals at a region were iron-reduction is developed and methane accumulation observed, possibly according to a DIET scheme.

MATERIALS AND METHODS

Research Site

The studied site is situated at a flood plain of the Tietê River, in São Paulo - SP, Brazil. The area contains a series of anthropogenic deposits ($\sim$4 m) that overlies Quaternary fluvial sediments ($\sim$6 m) and Neogene sandstones. The entire site was formerly used as a large drying pool for dredged sediments when a nearby channel was opened. The sediments settled in the pool kept under anoxic conditions the organic-rich sediments of the fluvial plain inducing methanogenic processes and methane trapping within sandy lenses at different depths of the section. Two main methane pockets were sampled along three multilevel monitoring wells, each one with 15 gas and water sampling ports 0.6 m spaced down to 8.6 m in the Quaternary section (Mendonça et al., 2015a). Continuous samples of direct-push coring were analyzed for total content of organic carbon and grain size laser diffraction Mendonça et al. (2015a). The trapped pockets of biogas were identified within a thick (approximately 6 m) layer of organic-rich sediments, with organic carbon up to 40% in weight. The pockets of methane were confirmed by direct gas sampling from the multilevel monitoring wells (**Figure 1**). The shallower accumulation (top at $\sim$2.5 m) has pressure equilibrated to the atmosphere, while the deeper gas reservoir (depth $\sim$6 m) is overpressured to about 0.4–0.5 kPa above the atmosphere. Gas composition in both reservoirs is enriched in CH_4, about 37–45% of CO_2 to 55–63% CH_4, with traces of H_2S ($\sim$30 ppm). The piezometric surface is relatively flat, with a hydraulic gradient of 0.0082 towards the river
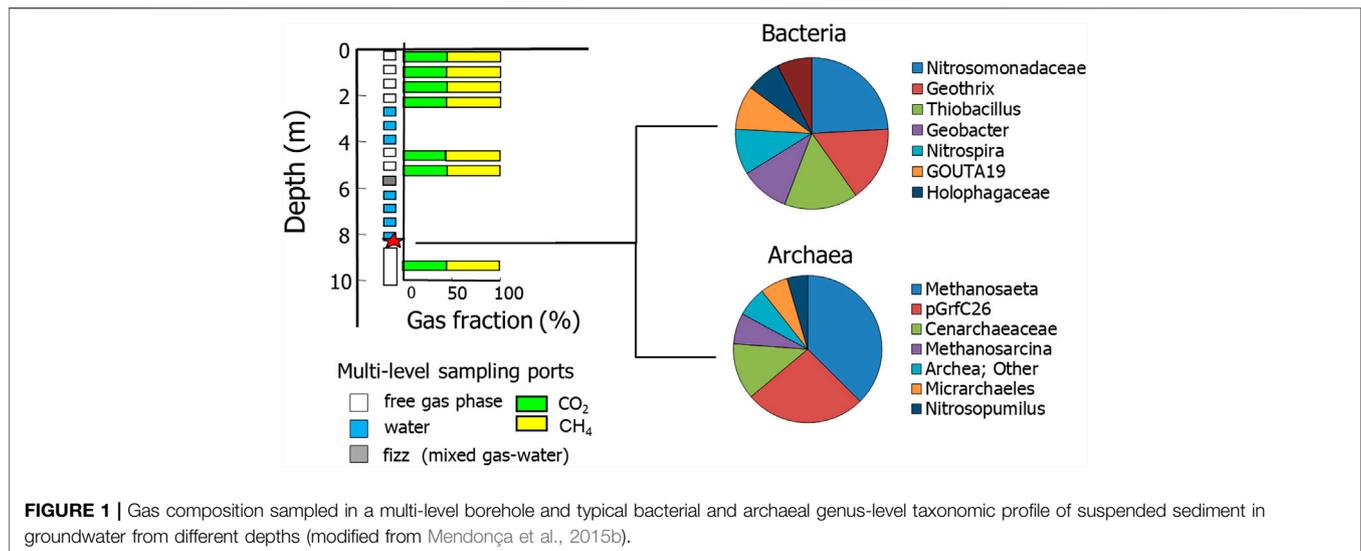
FIGURE 1 | Gas composition sampled in a multi-level borehole and typical bacterial and archaeal genus-level taxonomic profile of suspended sediment in groundwater from different depths (modified from Mendonça et al., 2015b).

channel. High permeability (12–62 cm day^{-1}) of the surface anthropogenic layer does not work as an efficient sealing unit for gas pockets volumes reaching the vadose zone but it facilitates water recharge and removal of gas in this zone as the water infiltrates. A monthly based ERT (Earth Resistivity Tomography) imaging recognized one episode with methane release and paths for water infiltration during rainy periods (Mendonça et al., 2015b).

Sediments recovered from groundwater sampled from the multi-wells underwent microbial analysis. Groundwater sampled from the multi-wells underwent microbial analysis. Procedures for microbial DNA extractions, bacterial and archaeal pyrosequencing, and sequence analysis are described in Mendonça et al. (2015b). It was found that the methane-producing archaea *Methanosaeta* are ubiquitous in the environment and probably generates the methane and carbon dioxide gas pockets trapped beneath impervious layers (**Figure 1**). The distribution of methanogens is well correlated with the methane pockets and higher levels of acetate. *Methanosaeta* species have high affinity for acetate (Lee et al., 2014) and are ubiquitous in many natural environments. *Methanosaeta* species are also capable of direct interspecies electron accepting from some *Geobacter* species for the reduction of carbon dioxide to methane (Rotaru et al., 2014b). Based on these findings we undertook a sampling regime of the recovered cores for magnetic properties characterization to identify if there is a relationship between methane production within gas pockets and the production of biogenic magnetic minerals in soils at the same horizons.

Magnetic Properties Characterization

Magnetic properties of soils and rocks are strongly dependent upon magnetic carrier grain size, which are classified as multi domain (MD), stable single domain (SSD), (e.g. up to 50 nm for magnetite), pseudo single domain (PSD) or "*vortex*" structure. Magnetic particles formed by dissimilatory iron-reducing bacteria are typically ultrafine, as such generating mineral carriers with superparamagnetic properties, (e.g. ultrafine magnetite or greigite) from reducing Fe(III) minerals from background geological media. To characterize the magnetic properties within and in the vicinity of the methane pockets 21 sediment samples from direct pushing coring (every 0.5 m, from 0.5 to 10.5 m deep) were analysed with focus on their superparamagnetic content, by using frequency dependent susceptibility (FDS) and superparamagnetic concentration and dipole moment (SPCDM) analysis.

Thermomagnetic Curve

In this analysis, magnetic susceptibility changes as a function of temperature are recorded. The high temperature protocol consists of measurements during the heating stage, from room temperature to approximately 700 °C and then repeating measurements while the sample cools to room temperature. High temperature curves are useful to identify changes of mineral phase that take place at specific temperatures, (e.g. Curie temperature T_C or Néel temperature T_N). T_C marks the sudden loss of magnetization when a ferri- or ferro-magnetic mineral becomes paramagnetic in temperatures $T > T_C$. For magnetite, $T_C \sim 580$ °C. T_N is the analogous of the Curie temperature in antiferromagnetic minerals such as hematite ($T_N \sim 675$ °C), where the mineral becomes paramagnetic at temperatures $T > T_N$ (Dunlop and Özdemir, 2001).

Thermomagnetic curves can also show magnetic carrier size effect, such as the Hopkinson peak (sudden increase of susceptibility temperature until a peak reached before T_C). Özdemir and Dunlop (2014) reported a systematic trend of the Hopkinson's peak height with magnetic grain size for natural magnetite samples. Also recognizable is mineral phase transformations as the sample is heated and cooled. In this case, the heating and cooling curves are distinguishable from one another and are said to be irreversible, revealing mineralogical transformations caused by dehydration or change in the sample redox state.

The measurements presented in this work were taken with Kappabridge KLY-4S at USPMAG (University of São Paulo), at the heating rate of 0.2 °C/s under inert Ar atmosphere.

Magnetic Hysteresis

Hysteresis cycles are designed to observe the ability of a ferromagnetic material to acquire permanent magnetization under an external magnetic field. This feature is usually investigated by first applying a strong field magnetic (H) so that the magnetization (M) is saturated. As H is then decreased to zero, M does not fall to the origin. If the field increases in the opposite direction, M gradually falls to zero to then reverse again as the saturation magnetization is reached. Repeated cycling of H traces out the *hysteresis loop*.

The standard hysteresis parameters *Mr*, *Ms*, *Hc*, and *Hcr* (where *Mr* is the saturation remanence, *Ms* is the saturation magnetization, *Hc* is the coercive force, and *Hcr* is the coercivity of remanence) represent the bulk magnetic properties of the sample and are often used to characterize geological samples. Low coercivity materials will produce hysteresis loops of rectangular shape and mixtures of minerals with different coercivities may produce constricted hysteresis loops that are narrow in the middle section but wider above and below this region (wasp-waisted) (Tauxe et al., 1996, 2002).

The analysis of hysteresis loops at different temperatures may reveal changes in the magnetic domain state for the magnetic minerals. Magnetic grains below a certain particle size, for example, do not preserve magnetic remanence above a critical temperature, when the superparamagnetic condition is activated (Dunlop and Özdemir, 2001).

We used the Physical Properties Measurement System (PPMS) Quantum Design using a vibrating sample magnetometry (VSM) to record hysteresis loops at 300, 25, 10 and 5 K and maximum external field of approximately 5×10^4 Oe.

First-Order Reversal Curves (FORC)

FORC diagrams (Pike et al., 1999; Roberts et al., 2000) provide further magnetic minerals and domain states characterization and the extent of magnetostatic interactions. FORC measurements start by saturating a sample in a strong positive field *Hr*, followed by changing the field to a negative field *Hr* and then sweeping it back to *Hr*. The difference between successive FORCs arises from irreversible magnetization changes that occur between successive reversal fields. FORCs distributions are interpreted in terms of the coercivity distribution and the interaction field distribution.

For example, an assemblage of noninteracting single domain particles produces closed concentric contours with negligible vertical spread of the FORC distribution, in contrast with the closed concentric contours with high vertical spread produced by interacting single domain particles. The superparamagnetic behavior is dominant in the FORC distribution when the measurement time is comparable to the relaxation times of particles near the SP-SSD threshold size (Pike et al., 2001). Multidomain particles produce a different feature in the FORC diagram, where the magnetic interactions among domain walls

produce asymmetric contours, which make it straightforward to discriminate these particles.
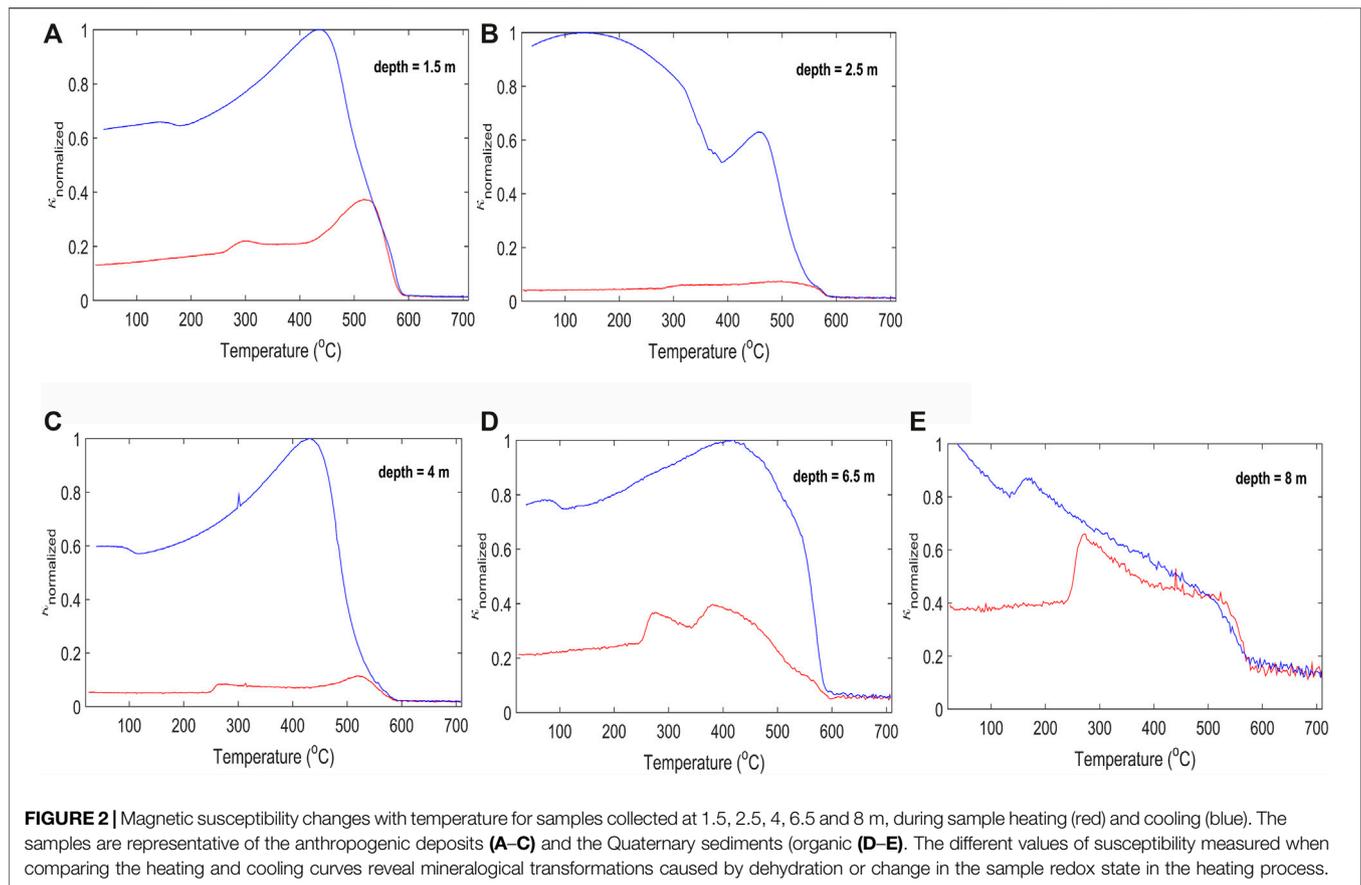
Frequency Dependent Susceptibility (FDS)

FDS aims to quantify the SP-SSD response in terms of grain size variation able to explain the dependence of the magnetic susceptibility with grain size fining from a reference SSD characteristic volume. This formulation is based on the Debye relaxation model (Ustra et al., 2018) by considering measurements with three-frequency susceptibilimeters usually employed to characterize superparamagnetic contents in soil and rock magnetism. According to this model, the in-phase (or real) magnetic susceptibility $\chi_r = \chi(f)$ for an assemblage of uniform magnetic carrier is $\chi_r = \chi_h + \Delta\chi \frac{1}{1+(2\pi f \tau)^2}$. where χ_h is the FDS high-frequency limit, $\Delta\chi = \chi_l - \chi_h$ with χ_l as its corresponding low-frequency limit and τ is relaxation time constant. For measurements with a set of at least three frequencies f, (e.g. 976, 3,904 and 15,616 Hz as for the MFK1-FA Kappabridge susceptibility meter) the FDS data allow solving for unknown parameters $(\chi_h, \Delta\chi, \tau)$ according to a constrained, non-linear data-fitting procedure (Ustra et al., 2019). Once estimated, such model parameters are used to determine the transition parameter $F_t = \chi_l/\chi_h = v/v_c$, that relates the mean volume v for the particle assemblage with respect to a characteristic volume $v_c = \frac{2k_B T}{\mu_0 H_K M_S}$.

Standing for the respective mineral grains in the SP-SSD transition, in which M_S is the sample saturation magnetization [Am^{-1}], k_B 1,38 $\times 10^{-23}$ [JK^{-1}] is the Boltzmann constant and T [K] is the temperature H_K [Am^{-1}]is the sample macroscopic coercivity and $\mu_0 = 4\pi \times 10^{-7}$ [Hm^{-1}] is the free space permeability. The quantity F_t^{-1}, such that $v_c = F_t^{-1}v$, can be regarded as a fining proxy since it expresses how much the particles go finer having as reference the characteristic volume for the grain. As discussed by Ustra et al. (2019) the determination of volume v according to the Neel's model $v = v_c \ln(\tau/\tau_0)$ is inaccurate using inferences for τ from data sets with three-frequencies only. Characteristic time τ_0 is a time-factor varying from 10^{-12} to 10^{-8} s (Dormann et al., 1996; Worm 1999). We use the MATLAB program *FDS_inv.m* (Ustra et al., 2019) to invert the three-frequency dataset acquired with Kappabridge MK1 at LabCore (University of São Paulo).

Superparamagnetic Concentration and Dipole Moment (SPCDM)

The SPCDM procedure developed by Leite et al. (2018) is based on Neél's model for superparamagnetism for which sample magnetization $M(B_i, T)$ is dependent of the external applied field (B_i) and temperature $M(B_i, T) = M_S L\left(\frac{\mu B_i}{k_B T}\right)$ in which μ is the mean moment of dipole [Am^2] of the magnetic carrier composing the sample; B_i is the external magnetic field applied to the sample, L is the Lagrange function such that $L(\alpha) = \coth(\alpha) - 1/\alpha$. The magnetization is such that $M_S = \eta\mu$, the term η [m^{-3}] expressing the concentration (number of particles per volume) of the magnetic carriers. For a sample with density ρ [kgm^{-3}], the mass concentration of the magnetic

FIGURE 2 | Magnetic susceptibility changes with temperature for samples collected at 1.5, 2.5, 4, 6.5 and 8 m, during sample heating (red) and cooling (blue). The samples are representative of the anthropogenic deposits **(A–C)** and the Quaternary sediments (organic **(D–E)**. The different values of susceptibility measured when comparing the heating and cooling curves reveal mineralogical transformations caused by dehydration or change in the sample redox state in the heating process.

carriers is obtained by η/ρ. The moment of dipole of the particle is such that $\mu = v\sigma_S$ where σ_S is the magnetization saturation for the magnetic carrier. The SPCDM procedure isolates the superparamagnetic contribution $M(B_i, T)$ by applying a set of external fields $B_i (i = 1 : 17)$ B_i ranging from 5 to 340 mT, by using a precise MicroMag3900 magnetometer, at USPMAG (University of São Paulo). These magnetization values provide unknown parameters (M_S, μ) from which estimates about particle concentration $(\eta = M_S/\mu)$ and particle volume $(v = \mu/\sigma_S)$ can be achieved. For volume estimates, the magnetization of pure magnetite can be assumed in most cases. In summary, the SPCDM provides saturation magnetization (M_S), the particle moment of dipole μ and, from these, particle concentration η [m^{-3}] and grain volume v, if saturation magnetization σ_S for mineral carrier is known.
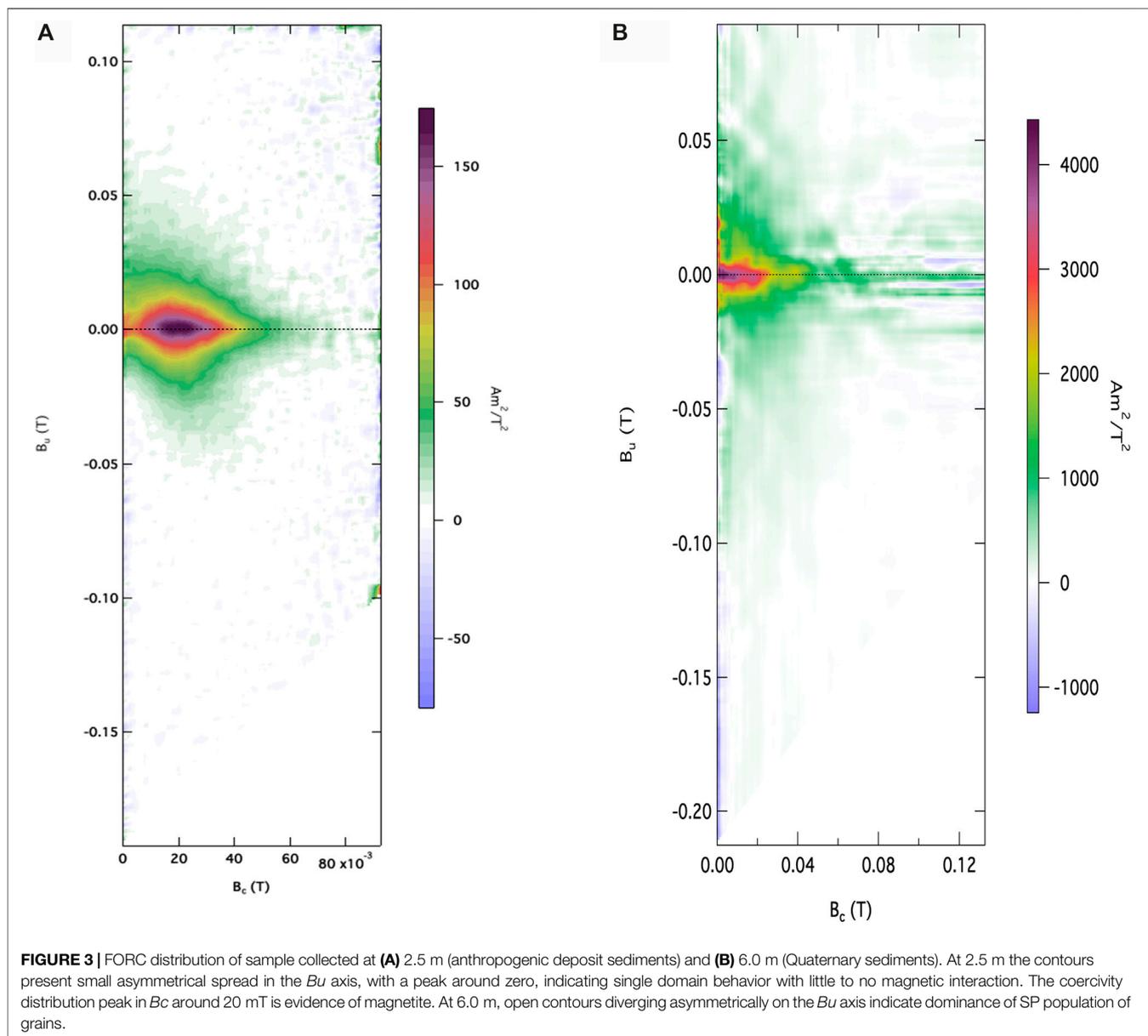
RESULTS AND DISCUSSION

The thermomagnetic measurements presented in **Figure 2** served as a preliminary analysis to identify the magnetic mineralogy diversity at the site. All heating curves captured the magnetic susceptibility increase above 250–300 ˚C, indicating transformations of iron (hydr)oxides under a reducing atmosphere (Hanesch et al., 2006). While heating, the

magnetic susceptibility increases with temperature to around 400–580 ˚C, followed by a significant loss of magnetization, indicating the occurrence of magnetite. The magnetic susceptibility increase indicates transformations of paramagnetic or clay minerals into magnetite (Roberts, 2015).

It is possible that ferrihydrite is being converted to magnetite, a common product of bacterial Fe(III) hydroxide reduction. The precipitation of magnetite in ferrihydrite reduction by dissimilatory Fe(III)-reducing microorganisms has been reported by several studies, (e.g. Lovley et al., 1987; Vali et al., 2004; Coker et al., 2008; Zhuang et al., 2015).

Even though magnetite is visible in the irreversible thermomagnetic curves, the presence of magnetite in the soils, prior the transformation of ferrihydrite into magnetite is verified in the FORC diagrams. **Figure 3A)** shows a clear SD-like behavior on 2.5 m (anthropogenic sediments) with small asymmetrical spread (higher towards the positive area) in the *Bu* axis, peaking around zero, indicating little to no magnetic interaction. The coercivity distribution peak in *Bc* is around 20 mT, evidence of magnetite, in accordance to the thermomagnetic curves. **Figure 3B)** shows the FORC diagram from the sample collected at 6 m (Quaternary sediments). A maximum coercivity peak close to the origin at around 5mT indicates a prevalent reversible component of magnetization (Sagnotti and Winkler, 2012), with open contours diverging asymmetrically on the *Bu* axis, showing resemblance to SP dominated population of
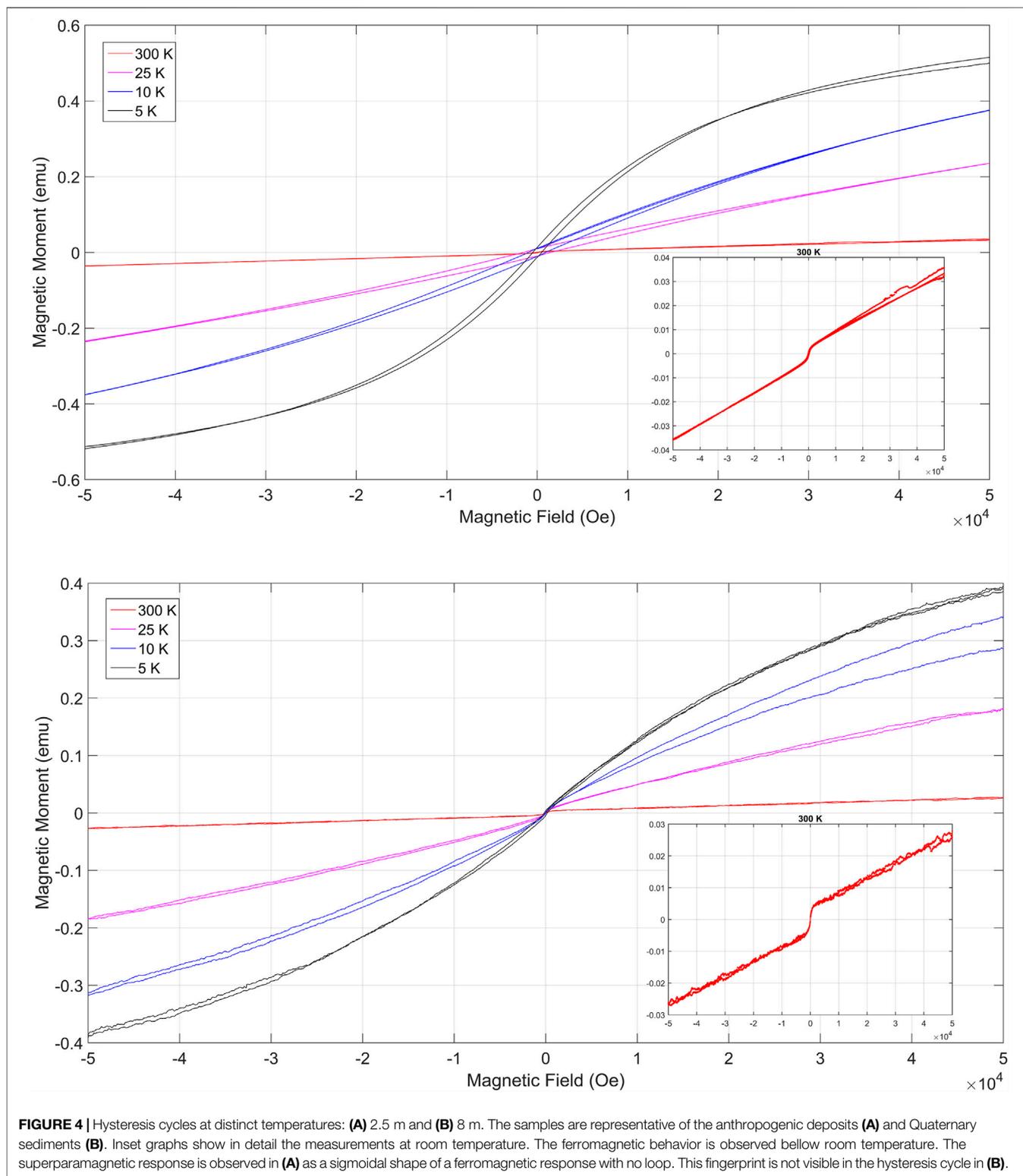
FIGURE 3 | FORC distribution of sample collected at **(A)** 2.5 m (anthropogenic deposit sediments) and **(B)** 6.0 m (Quaternary sediments). At 2.5 m the contours present small asymmetrical spread in the *Bu* axis, with a peak around zero, indicating single domain behavior with little to no magnetic interaction. The coercivity distribution peak in *Bc* around 20 mT is evidence of magnetite. At 6.0 m, open contours diverging asymmetrically on the *Bu* axis indicate dominance of SP population of grains.

grains (Roberts et al., 2014). The FORC also shows strong interaction fields (*Bu*) spreading until coercivities of 40 mT.

Samples collected at depths of 2.5 and 8 m were submitted to hysteresis cycles taken at distinct temperatures (**Figures 4A–C**, respectively). Below room temperature, the magnetization processes are irreversible and produces the ferromagnetic hysteresis loop. However, **Figures 4A,B** (2.5 m) and (8.0 m) capture the magnetic carrier's inabilities to sustain magnetization at room temperature (300 K, also shown as insets graphs), producing a superparamagnetic response of the sigmoidal shape of a ferromagnetic response, but losing the loop.
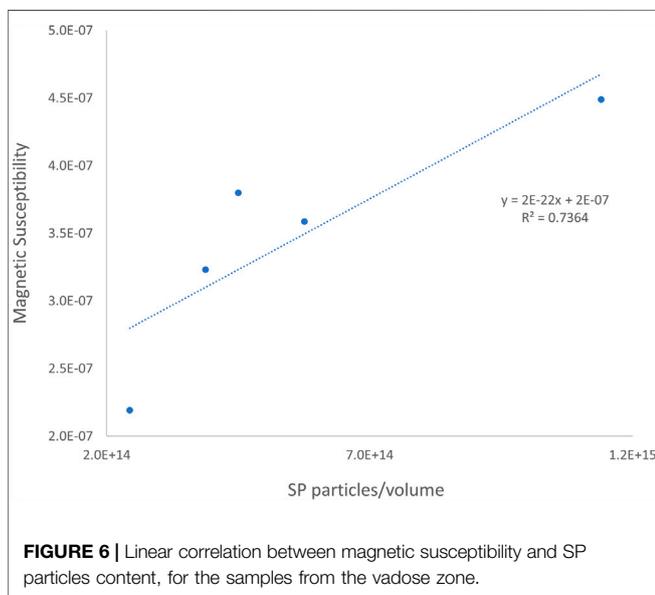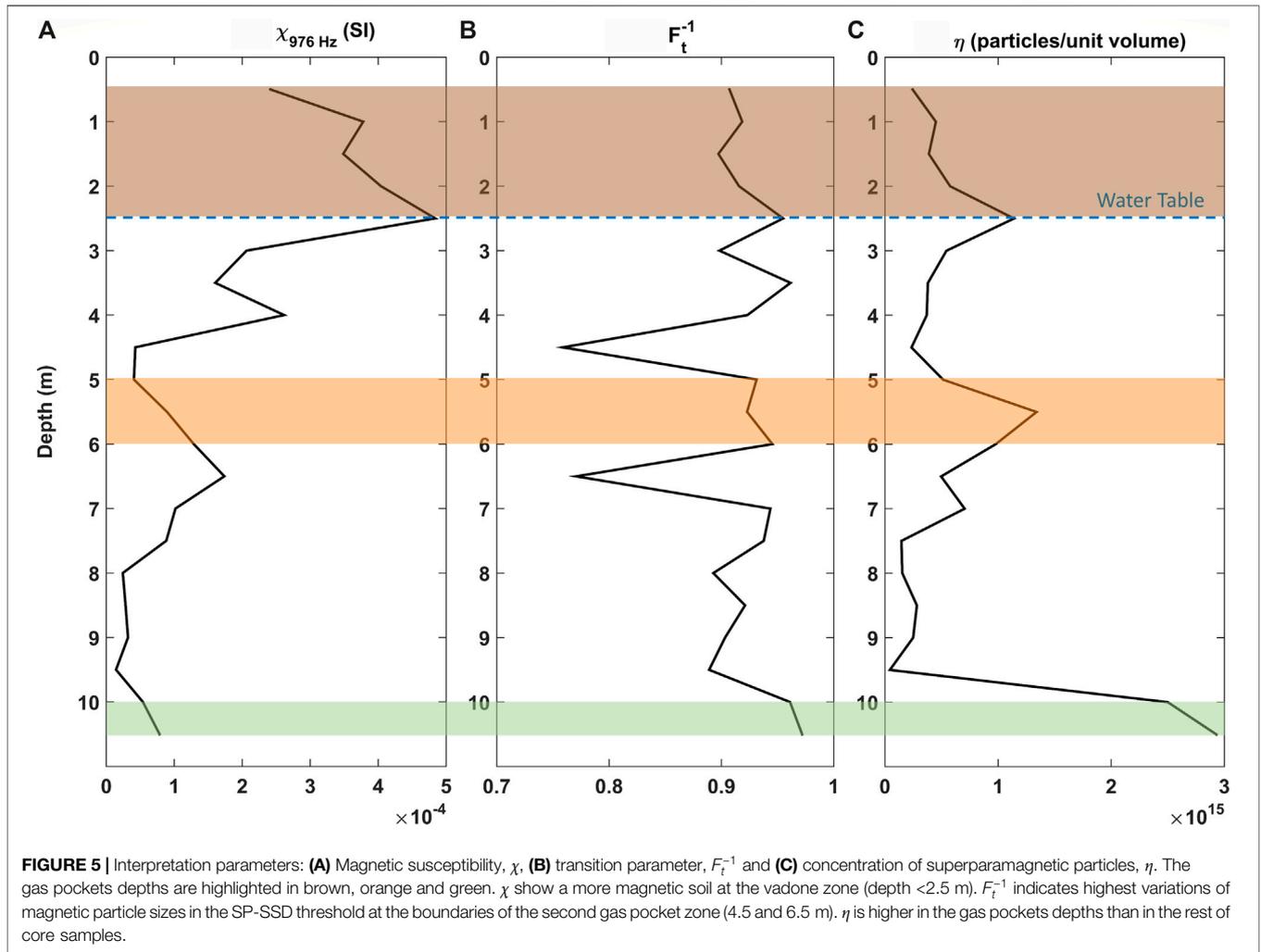
With evidence of SP-SSD particles in the magnetic particles assemblages, quantitative interpretation techniques based on the

SP-SSD magnetic response were applied (see **Supplementary material** for individual FDS and SPCDM analysis). **Figure 5** shows the depth profiles of the measured magnetic susceptibility, F_t^{-1} obtained from FDS measurements and superparamagnetic particles concentration, η. Magnetic susceptibility measurements (**Figure 5A**) show that the shallower portion of the soil is more magnetic and MS decreases with depth. The high MS in the uppermost 2.5 m is attributed to the unsaturated sediments magnetic properties. The maximum value of magnetic susceptibility is observed at 2.5 m, a known zone of gas pocket. Even though magnetic susceptibility decreases with depth, around 6.5 m it increases again, at a depth coincident with the second gas pocket zone. The parameter F_t^{-1}

FIGURE 4 | Hysteresis cycles at distinct temperatures: **(A)** 2.5 m and **(B)** 8 m. The samples are representative of the anthropogenic deposits **(A)** and Quaternary sediments **(B)**. Inset graphs show in detail the measurements at room temperature. The ferromagnetic behavior is observed bellow room temperature. The superparamagnetic response is observed in **(A)** as a sigmoidal shape of a ferromagnetic response with no loop. This fingerprint is not visible in the hysteresis cycle in **(B)**.

(**Figure 5B**), an estimation of the SP-SSD size variations, reveals that magnetic particles present a more significant frequency effect at 4.5 and 6.5 m. We interpret that magnetic carriers size variations in the SP-SSD threshold are more significant at these two depths,

which is at the boundary of the second gas pocket zone. The superparamagnetic particles concentration (SP concentration) profile (**Figure 5C**) shows two peaks, which agree with the gas pockets depths (0.5–2.5, 5–6 and 10.5 m).

FIGURE 5 | Interpretation parameters: **(A)** Magnetic susceptibility, χ, **(B)** transition parameter, F_t^{-1} and **(C)** concentration of superparamagnetic particles, η. The gas pockets depths are highlighted in brown, orange and green. χ show a more magnetic soil at the vadone zone (depth <2.5 m). F_t^{-1} indicates highest variations of magnetic particle sizes in the SP-SSD threshold at the boundaries of the second gas pocket zone (4.5 and 6.5 m). η is higher in the gas pockets depths than in the rest of core samples.

FIGURE 6 | Linear correlation between magnetic susceptibility and SP particles content, for the samples from the vadose zone.

The high MS values are not always in agreement with high SP particles shown by η, demonstrating that increasing content of SP ferrimagnetic particles alone cannot account for the variations of magnetic susceptibility of all samples. This apparent contradiction results from the limitations of both the FDS and the SPCDM methods. The FDS method captures a relaxation from magnetic particles within the SP-SSD threshold, in the 976–15,616 Hz AC field frequency range. On the other hand, the SPCDM captures faster relaxations, which are produced by finer particles (higher relaxation frequencies).

In this study, both methods were complementary, delimiting a zone of increasing the abundance SP-SSD particles (high F_t^{-1} and low η) and a zone of mostly SP particles (low F_t^{-1} and high η).

In the unsaturated zone, from 0.5 to 2.5 m, we believe that superparamagnetic particles are formed in a different process that will not be discussed in this work, where the grain size is not affected. The linear correlation between MS and η shown in **Figure 6** evidence that η follows the same pattern as
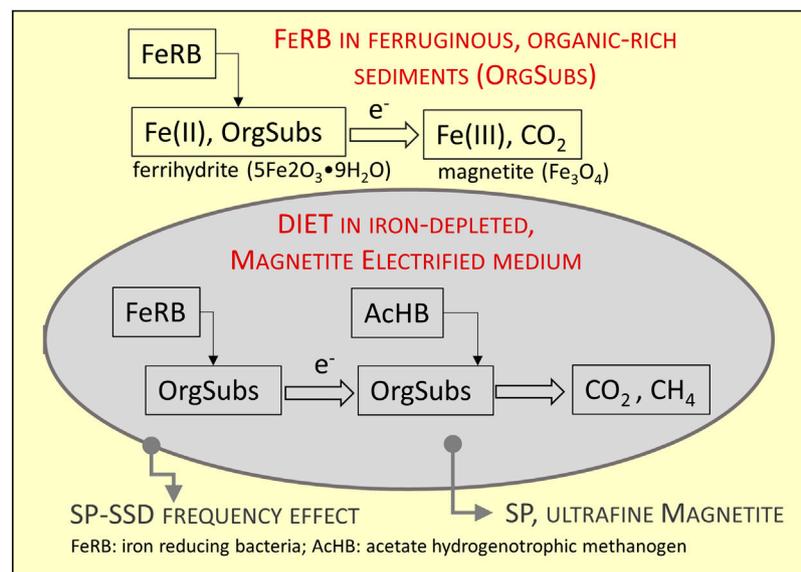
FIGURE 7 | Conceptual model illustrating the magnetic signatures observed across the methane pockets. The transformation of ferrihydrite into magnetite by iron reducing bacteria and the electron transfer to methanogens archaea. The DIET zone in this case is identified by a region of high SP content, surrounded by coarser particles within the SP-SSD threshold.

magnetic susceptibility within this anthropogenic layer, suggesting the magnetic response of this portion is dominated by the superparamagnetic particles. F_t^{-1} closer to one supports the interpretation that these depths are dominated by the superparamagnetic particles. When superparamagnetic particles are predominant, they dominate the susceptibility and SPCDM signals, but the frequency effect is little because there are little variations of the grain size distribution of the sample. In terms of bio-precipitation, this may be reflecting that most of the Fe-bearing particles are being used by microorganisms.

Even though magnetic signatures are a result of the magnetic grain sizes, this investigation approach does not aim to estimate the magnetic grain sizes and rather seek for these grains fingerprints. Moreover, the complex history of the site reminds us to expect an assemblage of grain sizes. This aspect enhances the usefulness of our quantitative interpretation procedures, which isolates and quantifies the ultrafine content.

In general, the distribution of SP minerals correlates well with the detected methanogens, suggesting that the SP particles of magnetite at these depths are anaerobically produced by iron-reducing dissimilatory microorganisms such as, *Geobacter* and *Geothrix*. There may be further syntrophy with methanogens such as *Methanosaeta* where Geobacter can further be involved in the DIET mechanism. Microbial analysis (**Figure 1**) supports the hypothesis of DIET as the methane producing mechanism at depths where superparamagnetic particles achieve highest concentrations. We propose a conceptual model of magnetic particles size range associated with the DIET hypothesis. **Figure 7** illustrates the transformation of ferrihydrite into magnetite by

iron reducing bacteria and the electron transfer to methanogens archaea. The DIET zone in this case is identified by a region of high SP content, surrounded by coarser particles within the SP-SSD threshold.

Other non-DIET reactions with Fe(III) reducing bacteria such as *Geothrix* with may also have a role in the production of magnetite (Klueglein et al., 2013) and there may be some syntrophy with *Methanosaeta* (Sutcliffe et al., 2018).

CONCLUSION

Magnetic properties measurements revealed the ultrafine magnetic particles occurrence in a brownfield site. The distribution of superparamagnetic concentration correlates well with the detected methanogens in gas pockets, suggesting that the microbial activity producing methane is producing these ultrafine particles, different from the magnetic particles produced at other depths. The results presented here support the use of environmental magnetism techniques to investigate biogeochemical processes of anaerobic microbial activity. Possibly, this kind of superparamagnetic fingerprint can be found in non-active methanogenic basins but recorded by magnetic mineralogy once preserved.

DATA AVAILABILITY STATEMENT

The raw data supporting the conclusions of this article will be made available by the authors, without undue reservation.

AUTHOR CONTRIBUTIONS

AU conducted the magnetic susceptibility measurements (frequency and temperature dependence), and conducted the multi-frequency analysis. AU has been studing the site for many years and for this study she planned the magnetic investigation and interpreted the results with the co-authors. CA was the project's PI and contributed discussing the results and writing/revising many parts of the manuscript. AL conducted the magnetizations decay and FORCs and MR conducted the hysteresis measurements. FORC and hysteresis were also supervised and discussed with MM. GT, an undergraduate student, conducted the thermomagnetic measurements. RD participated in the research at the site colaborating with the microbiological analysis. The results were discussed with all co-authors, who also wrote/revised the manuscript.

REFERENCES

Bryant, M. P., Wolin, E. A., Wolin, M. J., and Wolfe, R. S. (1967). Methanobacillus omelianskii, a symbiotic association of two species of bacteria. *Arch. Mikrobiol.* 59, 20–31. doi:10.1007/BF00406313

Byrne, J. M., Klueglein, N., Pearce, C., Rosso, K. M., Appel, E., and Kappler, A. (2015). Redox cycling of Fe(II) and Fe(III) in magnetite by Fe-metabolizing bacteria. *Science* 347, 1473–1476. doi:10.1126/science.aaa4834

Chen, S., Rotaru, A. E., Liu, F., Philips, J., Woodard, T. L., Nevin, K. P., et al. (2014b). Carbon cloth stimulates direct interspecies electron transfer in syntrophic co-cultures. *Bioresour. Technol.* 173, 82–86. doi:10.1016/j.biortech.2014.09.009

Chen, S., Rotaru, A. E., Shrestha, P. M., Malvankar, N. S., Liu, F., Fan, W., et al. (2014a). Promoting interspecies electron transfer with biochar. *Sci. Rep.* 4, 5019. doi:10.1038/srep05019

Christensen, T. R. (2010). *Wetlands in methane and climate change.* London, United Kingdom: Earthscan Ltd.

Coker, V. S., Bell, A. M. T., Pearce, C. I., Pattrick, R. A. D., Van der Laan, G., and Lloyd, J. R. (2008). Time-resolved synchrotron powder X-ray diffraction study of magnetite formation by the Fe(III)-reducing bacterium Geobacter sulfurreducens. *Am. Mineral.* 93 (4), 540–547. doi:10.2138/am.2008.2467

Dormann, J. L., D'Orazio, F., Lucari, F., Tronc, E., Prené, P., Jolivet, J. P., et al. (1996). Thermal variation of the relaxation time of the magnetic moment of gamma -Fe2O3 nanoparticles with interparticle interactions of various strengths. *Phys. Rev. B Condens. Matter.* 53 (21), 14291. doi:10.1103/physrevb.53.14291

Dunlop and Özdemir, D. J. O. (2001). *Rock magnetism: fundamentals and Frontiers.* Cambridge Univ. Press.

Hanesch, M., Stanjek, H., and Petersen, N. (2006). Thermomagnetic measurements of soil iron minerals: the role of organic carbon. *Geophys. J. Int.* 165, 53–61. doi:10.1111/j.1365-246x.2006.02933.x

Kato, S., Hashimoto, K., and Watanabe, K. (2012). Microbial interspecies electron transfer via electric currents through conductive minerals. *Proc. Natl. Acad. Sci. U.S.A.* 109, 10042–10046. doi:10.1073/pnas.1117592109

Klueglein, N., Lösekann-Behrens, T., Obst, M., Behrens, S., Appel, E., and Kappler, A. (2013). Magnetite formation by the novel Fe(III)-reducingGeothrix fermentansStrain HradG1 isolated from a hydrocarbon-contaminated sediment with increased magnetic susceptibility. *Geomicrobiol. J.* 30, 863–873. doi:10.1080/01490451.2013.790922

Lee, J., Hwang, B., Koo, T., Shin, S. G., Kim, W., and Hwang, S. (2014). Temporal variation in methanogen communities of four different full-scale anaerobic digesters treating food waste-recycling wastewater. *Bioresour. Technol.* 168 (3), 59–63. doi:10.1016/j.biortech.2014.03.161

ACKNOWLEDGMENTS

SUPPLEMENTARY MATERIAL

The Supplementary Material for this article can be found online at: https://www.frontiersin.org/articles/10.3389/feart.2020.608387/full#supplementary-material.

Lee, J. H., Roh, Y., and Hur, H. G. (2008). Microbial production and characterization of superparamagnetic magnetite nanoparticles by Shewanella sp. HN-41. *J. Microbiol. Biotechnol.* 18, 1572–1577.

Leite, A. S., Mendonça, C. A., Moraes, P. L. A., and Ustra, A. T. (2018). A procedure for quantitative characterization of superparamagnetic minerals in environmental magnetism. *Geophys. J. Int.* 215 (3), 1974–1984. doi:10.1093/gji/ggy395

Li, Y., Zhang, H., Tu, C., and Luo, Y. (2018). Magnetic characterization of distinct soil layers and its implications for environmental changes in the coastal soils from the yellow river delta. *Catena* 162, 245–254. doi:10.1016/j.catena.2017.11.006

Liu, F., Rotaru, A. E., Shrestha, P. M., Malvankar, N. S., Nevin, K. P., and Lovley, D. R. (2015). Magnetite compensates for the lack of a pilin-associated c-type cytochrome in extracellular electron exchange. *Environ. Microbiol.* 17, 648–655. doi:10.1111/1462-2920.12485

Liu, F., Rotaru, A.-E., Shrestha, P. M., Malvankar, N. S., Nevin, K. P., and Lovley, D. R. (2012). Promoting direct interspecies electron transfer with activated carbon. *Energy Environ. Sci.* 5, 8982. doi:10.1039/c2ee22459c

Lovley, D. R., Stolz, J. F., Nord, G. L., and Phillips, E. J. P. (1987). Anaerobic production of magnetite by a dissimilatory iron-reducing microorganism. *Nature* 330, 252–254. doi:10.1038/330252a0

Lovley, D. R. (1991). "Magnetite formation during microbial dissimilatory iron reduction," in *Iron biominerals*. Editors R. B. Frankel and R. P. Blakemore (Berlin, Germany: Springer), 151–166. doi:10.1007/978-1-4615-3810-3_11

Lovley, D. R., Holmes, D. E., and Nevin, K. P. (2004). Dissimilatory Fe(III) and Mn(IV) reduction. *Adv. Microb. Physiol.* 49, 219–286. doi:10.1016/S0065-2911(04)49005-5

Lovley, D. R. (2011). Live wires: direct extracellular electron exchange for bioenergy and the bioremediation of energy-related contamination. *Energy Environ. Sci.* 4, 4896–4906. doi:10.1039/c1ee02229f

Lovley, D. R. (2017). Syntrophy goes electric: direct interspecies electron transfer. *Annu. Rev. Microbiol.* 71, 643–664. doi:10.1146/annurev-micro-030117-020420

Maher, B. A., and Taylor, R. M. (1988). Formation of ultrafine-grained magnetite in soils. *Nature* 336, 368–370. doi:10.1038/336368a0

Martins, G., Salvador, A. F., Pereira, L., and Alves, M. M. (2018). Methane production and conductive materials: a critical review. *Environ. Sci. Technol.* 52 (18), 10241–10253. doi:10.1021/acs.est.8b01913

Mendonça, C. A., Doherty, R., Fornaro, A., Abreu, E. L., Novaes, G. C., Fachin, S. J. S., et al. (2015a). Integrated earth resistivity tomography (ERT) and multilevel sampling gas: a tool to map geogenic and anthropogenic methane accumulation on brownfield sites. *Environ Earth Sci.* 74, 1217–1226. doi:10.1007/s12665-015-4111-6

Mendonça, C. A., Doherty, R., Amaral, N. D., McPolin, B., Larkin, M. J., and Ustra, A. (2015b). Resistivity and induced polarization monitoring with microbial ecology of biogas dynamics on a brownfield site. *Inter* 4 (3), SAB43–SAB56. doi:10.1190/INT-2015-0057.1

Moskowitz, B. M., Frankel, R. B., and Bazylinski, D. A. (1993). Rock magnetic criteria for the detection of biogenic magnetite. *Earth Planet Sci. Lett.* 120, 283–300. doi:10.1016/0012-821x(93)90245-5

Özdemir, Ö., and Dunlop, D. J. (2014). Hysteresis and coercivity of hematite. *J. Geophys. Res. Solid Earth* 119, 2582–2594. doi:10.1002/2013jb010739

Pike, C. R., Roberts, A. P., and Verosub, K. L. (1999). Characterizing interactions in fine magnetic particle systems using first order reversal curves. *J. Appl. Phys.* 85, 6660–6667. doi:10.1063/1.370176

Pike, C. R., Roberts, A. P., and Verosub, K. L. (2001). First-order reversal curve diagrams and thermal relaxation effects in magnetic particles. *Geophys. J. Int.* 145, 721–730. doi:10.1046/j.0956-540x.2001.01419.x

Roberts, A. P., Heslop, D., Zhao, X., and Pike, C. R. (2014). Understanding fine magnetic particle systems through use of first-order reversal curve diagrams. *Rev. Geophys.* 52 (4), 557–602. doi:10.1002/2014rg000462

Roberts, A. P. (2015). Magnetic mineral diagenesis. *Earth Sci. Rev.* 151, 1–47. doi:10.1016/j.earscirev.2015.09.010

Roberts, A. P., Pike, C. R., and Verosub, K. L. (2000). FORC diagrams: anew tool for characterizing the magnetic properties of natural samples. *J. Geophys. Res.* 105 (28), 461–475 .doi:10.1029/2000jb900326

Rotaru, A.-E., Shrestha, P. M., Liu, F., Shrestha, M., Shrestha, D., Embree, M., et al. (2014b). A new model for electron flow during anaerobic digestion: direct interspecies electron transfer to Methanosaeta for the reduction of carbon dioxide to methane. *Energy Environ. Sci.* 7, 408–415. doi:10.1039/c3ee42189a

Rotaru, A. E., Calabrese, F., Stryhanyuk, H., Musat, F., Shrestha, P. M., Weber, H. S., et al. (2018). Conductive particles enable syntrophic acetate oxidation between Geobacter and Methanosarcina from coastal sediments. *mBio* 9, e00226–18. doi:10.1128/mBio.00226-18

Rotaru, A. E., Shrestha, P. M., Liu, F., Markovaite, B., Chen, S., Nevin, K. P., et al. (2014a). Direct interspecies electron transfer between Geobacter metallireducens and Methanosarcina barkeri. *Appl. Environ. Microbiol.* 80, 4599–4605. doi:10.1128/AEM.00895-14

Sagnotti, L., and Winkler, A. (2012). On the magnetic characterization and quantification of the superparamagnetic fraction of traffic-related urban airborne PM in Rome, Italy. *Atmos. Environ.* 59, 131–140. doi:10.1016/j.atmosenv.2012.04.058

Shrestha, P. M., Rotaru, A. E., Aklujkar, M., Liu, F., Shrestha, M., Summers, Z. M., et al. (2013b). Syntrophic growth with direct interspecies electron transfer as the primary mechanism for energy exchange. *Environ Microbiol Rep.*, 5, 904–910. doi:10.1111/1758-2229.12093

Shrestha, P. M., Rotaru, A. E., Summers, Z. M., Shrestha, M., Liu, F., and Lovley, D. R. (2013a). Transcriptomic and genetic analysis of direct interspecies electron transfer. *Appl. Environ. Microbiol.* 79, 2397–2404. doi:10.1128/AEM.03837-12

Sieber, J. R., McInerney, M. J., and Gunsalus, R. P. (2012). Genomic insights into syntrophy: the paradigm for anaerobic metabolic cooperation. *Annu. Rev. Microbiol.* 66, 429–452. doi:10.1146/annurev-micro-090110-102844

Stams, A. J., and Plugge, C. M. (2009). Electron transfer in syntrophic communities of anaerobic bacteria and archaea. *Nat. Rev. Microbiol.* 7, 568–577. doi:10.1038/nrmicro2166

Summers, Z. M., Fogarty, H. E., Leang, C., Franks, A. E., Malvankar, N. S., and Lovley, D. R. (2010). Direct exchange of electrons within aggregates of an evolved syntrophic coculture of anaerobic bacteria. *Science* 330, 1413–1415. doi:10.1126/science.1196526

Sutcliffe, B., Chariton, A. A., Harford, A. J., Hose, G. C., Stephenson, S., Greenfield, P., et al. (2018). Insights from the genomes of microbes thriving in uranium-enriched sediments. *Microb. Ecol.* 75, 970–984. doi:10.1007/s00248-017-1102-z

Tauxe, L., Bertram, H. N., and Seberino, C. (2002). Physical interpretation of hysteresis loops: micromagnetic modeling of fine particle magnetite. *G-cubed* 3 (10), 1–22. doi:10.1029/2001gc000241

Tauxe, L., Pick, T., and Constable, C. (1996). Wasp-waists, pot-bellies, and superparamagnetism. *Journal of Geophysical Research B: Solid Earth* 101 (95), 571–583. doi:10.1029/95jb03041

Ustra, A., Mendonça, C. A., Leite, A., Jovane, L., and Trindade, R. I. F. (2018). Quantitative interpretation of the magnetic susceptibility frequency dependence. *Geophys. J. Int.* 213 (2), 805–814. doi:10.1093/gji/ggy007

Ustra, A., Mendonça, C., Leite, A., Jaqueto, P., and Novello, V. F. (2019). Low field frequency dependent magnetic susceptibility inversion. *Comput. Geosci.* 133, 104326. doi:10.1016/j.cageo.2019.104326

Vali, H., Weiss, B., Li, Y. L., Sears, S. K., Kim, S. S., Kirschvink, J. L., et al. (2004). Formation of tabular single-domain magnetite induced by Geobacter metallireducens GS-15. *Proc. Natl. Acad. Sci. U.S.A.* 101 (46), 16121–16126. doi:10.1073/pnas.0404040101

Wang, L. Y., Nevin, K. P., Woodard, T. L., Mu, B. Z., and Lovley, D. R. (2016). Expanding the diet for DIET: electron donors supporting direct interspecies electron transfer (DIET) in defined co-cultures. *Front. Microbiol.* 7, 236. doi:10.3389/fmicb.2016.00236

Worm, H.-U. (1999). Time-dependent IRM: a new technique for magnetic granulometry. *Geophys. Res. Lett.* 26 (16), 2557–2560. doi:10.1029/1999gl008360

Xiao, L., Liu, F., Liu, J., Li, J., Zhang, Y., Yu, J., et al. (2018). Nano-Fe3O4 particles accelerating electromethanogenesis on an hour-long timescale in wetland soil. *Environ. Sci. Nano* 5, 436–445. doi:10.1039/C7EN00577F

Xiao, L., Wei, W., Luo, M., Xu, H., Feng, D., Yu, J., et al. (2019). A potential contribution of a Fe(III)-rich red clay horizon to methane release: biogenetic magnetite-mediated methanogenesis. *Catena* 181, 104081. doi:10.1016/j.catena.2019.104081

Zhang, J., and Lu, Y. (2016). Conductive Fe3O4 nanoparticles accelerate syntrophic methane production from butyrate oxidation in two different lake sediments. *Front. Microbiol.* 7, 1316. doi:10.3389/fmicb.2016.01316

Zhao, Z., Li, Y., Yu, Q., and Zhang, Y. (2018). Ferroferric oxide triggered possible direct interspecies electron transfer between Syntrophomonas and Methanosaeta to enhance waste activated sludge anaerobic digestion. *Bioresour. Technol.* 250, 79–85. doi:10.1016/j.biortech.2017.11.003

Zhuang, L., Xu, J., Tang, J., and Zhou, S. (2015). Effect of ferrihydrite biomineralization on methanogenesis in an anaerobic incubation from paddy soil. *J. Geophys. Res. Biogeosci.* 120, 876–886. doi:10.1002/2014jg002893